Available online at www.sciencedirect.com
SCIENCE DIRECT®
International Journal of Heat and Fluid Flow 26 (2005) 431–439
International Journal of HEAT AND FLUID FLOW
www.elsevier.com/locate/ijhff

Control of confined nonpremixed flames using a microjet

Ashok Sinha [a], Ranjan Ganguly [a,b], Ishwar K. Puri [a,*]

[a] Department of Engineering Science and Mechanics, Virginia Polytechnic Institute and State University, 223 Norris Hall (0219), Blacksburg, VA 24061, USA
[b] Department of Power Engineering, Jadavpur University, Calcutta 700032, India

Received 14 April 2004; accepted 2 November 2004
Available online 19 December 2004

Abstract

Industrial burners, such as those used in materials processing furnaces, require precise control over the flame length, width, overall shape and other physical flame attributes. The mechanism used to control the flame topology should be relatively simple, safe, and devoid of an emissions penalty. We have explored the feasibility of hydrodynamic control of confined nonpremixed flames by injecting air through a high-momentum microjet. An innovative strategy for the control of flame shape and luminosity is demonstrated based on a high-momentum coaxial microjet injected along the center of a confined nonpremixed flame burning in a coflowing oxidizer stream. The introduction of the microjet shortens a nonpremixed flame and reduces the amplitude of the buoyancy-induced flickering. For a microjet-assisted flame, the flame length is more sensitive to the fuel flowrate than for laminar or turbulent nonpremixed flames. This provides greater flexibility for the dynamic control of their flame lengths.

Measurements of NO_x and CO emissions show that the method is robust. Effective flame control without an emissions penalty is possible over a large range of microjet velocities that significantly alter the flame shape. Since the influence of the microjet is primarily of a hydrodynamic nature, inert microjet fluids like recirculated exhaust gas can also be used in practical devices.
© 2004 Elsevier Inc. All rights reserved.

Keywords: Nonpremixed flame; Flame control; Jet entrainment

1. Introduction

Industrial burners, such as those used in materials processing furnaces, require precise control over the flame length, shape and other physical flame attributes. For instance Hanus and Hubo (1999) studied variable flame length burners required in the steel industry for the flame strengthening of steel. These burners allow control over the furnace heat transfer characteristics by varying the flame length and the heat release profile, as in Pesenti and Meunier (2000). The active control of flame length and shape is also desirable in other energy-intensive applications, such as glass and other melting furnaces, and in welding torches. Ideally, a control technique should not require sophisticated instrumentation or significant modifications to the burner hardware. There are potential pitfalls to altering the flame structure, such as an increase in undesirable flame emissions and a loss of flame stability. Therefore, the mechanism used to control the flame topology should be relatively simple (e.g., as compared to Lawton and Weinberg (1969) who applied an external electric field or Hertzberg (1977) who used acoustic forcing), safe, and devoid of an emissions penalty.

Thring and Newby (1953) and Becker et al. (1981) carried out several investigations characterizing the conditions that alter the flame shape and spread in both confined and nonconfined flames. Hydrodynamic effects at the burner exit are known to change the flame topology. Apart from flame shape and size, flame

* Corresponding author. Tel.: +1 540 231 2343; fax: +1 540 231 4574.
E-mail address: ikpuri@vt.edu (I.K. Puri).

0142-727X/$ - see front matter © 2004 Elsevier Inc. All rights reserved.
doi:10.1016/j.ijheatfluidflow.2004.11.001

flickering is another important physical parameter that has strong industrial relevance. Kimura (1965) characterized buoyant laminar jet flames with respect to gravity-induced flickering. Hamins et al. (1992) related the burner diameter, jet Reynolds number and fuel properties with the flickering behavior. For slot burners, Roper (1977) and Roper et al. (1977) identified three regimes of flame behavior: buoyancy controlled, transition, and momentum controlled depending on whether the Froude number was very small, of the order of unity, or very large. Heat and mass transport in flames established with extremely low velocity fuel jets on small burners can be dominated by molecular diffusion rather than by convection or buoyancy. Ban et al. (1994) observed that it is possible to almost eliminate the effect of gravity and produce a nearly spherical nonpremixed flame when the dimensionless Peclet number Pe (= ud/D, where D denotes the pertinent mass diffusivity) has a value smaller than five. Becker and Yamazaki (1978) performed a more extensive parametric investigation of micro-slot nonpremixed flames and determined that for low values of a diffusion-to-buoyancy parameter, the flame shape is buoyancy controlled. Momentum was shown to play a more dominant role in flames associated with low values of the diffusion-to-momentum ratio.

Recently, Ganguly and Puri (2004) demonstrated that a high-momentum fluid jet applied along the centerline of a nonpremixed flame burning in an unconfined quiescent environment (i.e., in absence of any coflow) can be used to control the flame topology and the fuel–air mixing. Using this method, it is possible to keep the fuel jet velocity unchanged in order to avoid liftoff and blowout, but achieve increased entrainment. Although the burning of a fuel jet in a quiescent environment has scientific relevance, most practical nonpremixed combustion applications involve confinement in which the oxidizer demand is met through a coflow. For many applications, e.g. wall-fired furnaces and dump combustors, the dimensions of confinement are several times larger than the burner diameter. Here, the flame characteristics are strongly influenced by the coflow. Therefore, a technique similar to that proposed by Ganguly and Puri (2004) for controlling the flame shape could prove useful for confined nonpremixed flames that are established with coflowing oxidizer streams.

2. Objective

We have explored the feasibility of hydrodynamic control of nonpremixed flames established in a large confinement in the presence of a coflow by injecting air through a high-momentum jet of sub-millimeter radius. We will refer to this jet as a microjet, although its dimension is relative and its purpose is to produce a relatively narrow high-velocity stream. The air microjet is applied along the center of a buoyant nonpremixed fuel stream that is surrounded by a coflowing stream of air. The resulting flame characteristics are investigated by varying the relative strengths of each of these three flows. Our objective is to enhance oxidizer entrainment from the coflowing stream in the flame and thus control the flame shape, flickering and luminosity. The flame structure is investigated by direct imaging, Schlieren and thermocouple measurements. We also measure the global CO and NO_x emissions to ascertain that the control method does not result in an emissions penalty.

3. Configuration

The burner assembly is schematically described in Fig. 1. It consists of three axially concentric cylinders. The inner radii of the three cylinders are 500 μm, 4.5 mm, and 21 mm, respectively. All three cylinders have a 1 mm wall thickness. A steady flow of the fuel (methane) emerges from the intermediate cylinder and the outer annulus supplies a steady coflow of air. An air microjet flow is applied through the central port. There are separate lines to the three ports and the gas flows are measured using calibrated rotameters under a regulated pressure at room temperature. There is a 170 mm diameter and 450 mm long confinement around the flame. Only the coflowing stream and the air microjet supply the oxidizer required for combustion.

Direct and Schlieren images of the flames are obtained at 30 fps with a CCD camera. The flickering frequency of a nonpremixed flame (unassisted by a microjet) is ~10 Hz. Flame height data are reconstructed by averaging a large number of sequential direct images. The flame temperatures are measured using a 0.2 mm R-type thermocouple. The thermocouple time constant is ~0.1 s. Each reported temperature is the rms value obtained from 300 temperature readings. The error bars in the temperature plots present the temperature variance at each location. Corrections are made to compensate for the radiation loss from the thermocouple bead (Azzoni et al., 1999). We did not observe any soot accumulation on the bead and, consequently, assumed a constant emissivity for the Pt–Rh bead. The flue gases from the confined flames are directed into a chimney where they are sampled (at a distance 900 mm above the burner exit) for NO_x and CO analyses. The NO_x analyzer is capable of measuring levels of the oxides of nitrogen from 0.1 to 5000 ppm. The CO analyzer is based on the 4.6 μm wavelength infrared radiation absorption by dry CO gas, and is capable of measurements in the range 1–100 ppm.

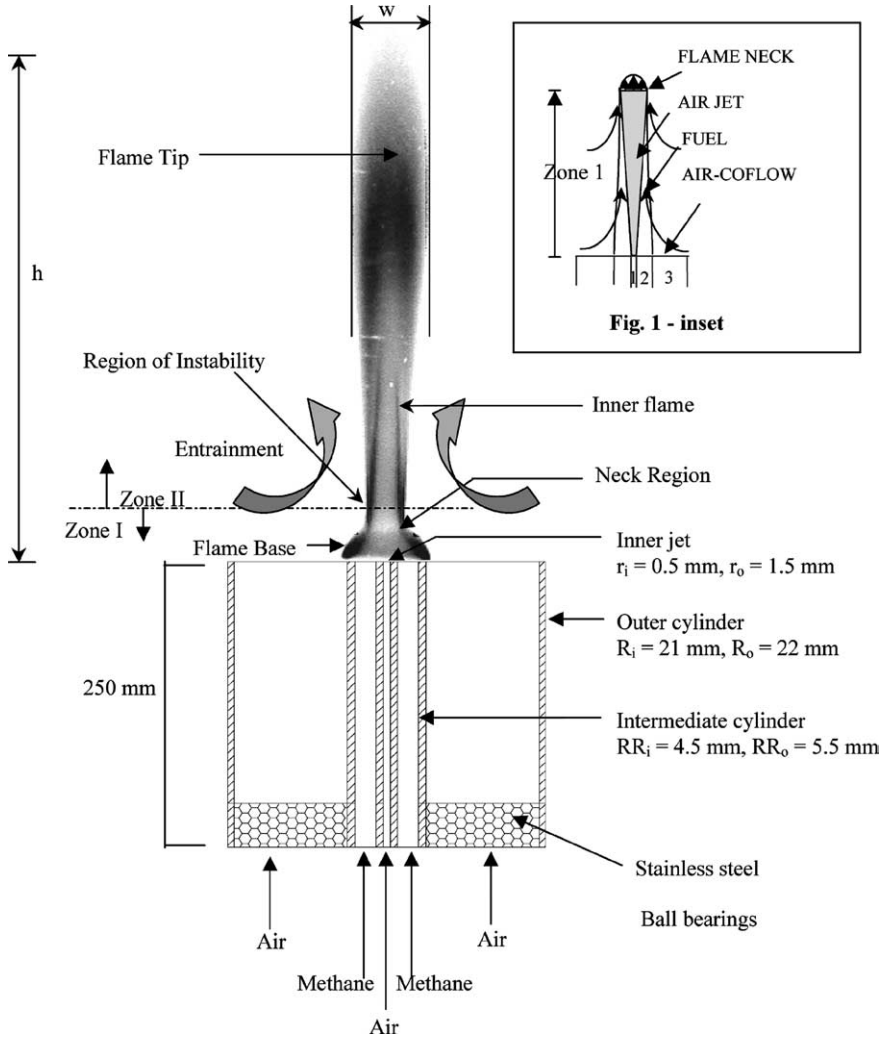

Fig. 1. Schematic burner configuration and a microjet-assisted flame (Flame (F) of Table 1).

4. Results and discussion

Fig. 2(A) presents a direct image of a nonpremixed flame in the absence of a microjet. The fuel stream exit velocity $v_f = 0.33$ m/s ($Re_d \sim 150$) and the air coflow velocity $v_c = 5.5$ m/s. The flame is characterized by buoyancy-induced flickering and a large luminosity that is indicative of soot formation. Air microjets are introduced for constant fuel flow and air coflow velocities for the flames shown in images (B)–(F). The microjet flowrates are reported in Table 1(panel a).

Until a microjet velocity v_j of ~10 m/s, the nonpremixed flame does not exhibit any significant change in its shape. When $v_j > 10$ m/s the flame height begins to diminish. Beyond $v_j = 13$ m/s (for microjet Reynolds numbers $Re_j > 2000$), a "flame neck" appears when the radial cross section of the luminous flame shows a constriction that divides the flame into an upstream Zone I and a downstream Zone II. Its formation is associated with a "fluttering" noise, which increases as the microjet velocity is raised. This sound originates due to local extinction and immediate reignition in the "flame neck" region. Below the neck, visual and Schlieren images confirm that the flame is steady and laminar in Zone I. However, the Zone II above the neck is not laminar. (These zones are also illustrated in Fig. 1). Images of Flames (C)–(F) in Fig. 2 show that as the microjet velocity is increased, the overall luminous flame height decreases and the flame neck location gradually moves upstream.

In absence of the microjet, the oxidizer supply to the confined nonpremixed flame occurs place mainly through cross-stream diffusion. A high momentum microjet applied at the center of the reacting flow alters the hydrodynamics. The central jet creates a low-pressure region close to the burner plane, inducing an inward radial advective flux of the oxidizer from the coflowing air stream. This is qualitatively described by the schematic of Fig. 1. Han and Mungal (2001) correlated the rate of entrainment with the mixing rate of

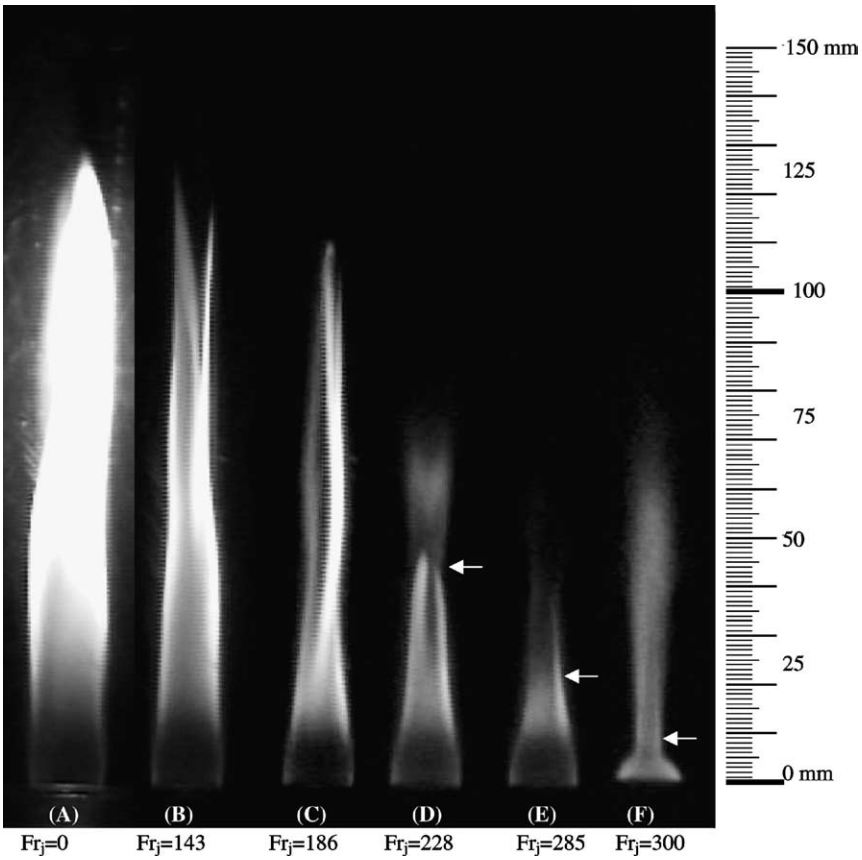

Fig. 2. The topologies of Flames (A) through (F) of Table 1(panel a) for which only the microjet velocities are changed. Microjet Froude number ($Fr_j = v_j/\sqrt{(r_i g)}$) values for a given fuel jet Froude number ($Fr_f = v_f/\sqrt{((R_i - r_o)g)} = 1.9$) compare the square root of the ratio of the microjet momentum to buoyancy.

Table 1
Operating conditions

		A	B	C	D	E	F
Panel a							
Microjet velocity (m/s)	v_j	0	10	13	16	20	21
Fuel jet velocity (m/s)	v_f	0.33	0.33	0.33	0.33	0.33	0.33
Coflow velocity (m/s)	v_c	5.5	5.5	5.5	5.5	5.5	5.5
Overflow equivalence ratio	ϕ[a]	0.025	0.025	0.025	0.025	0.025	0.025
Flame height (mm)	L_f	132	120	113	82	63	85

		G	H	I	J	K	L	M	N	O
Panel b										
Microjet velocity (m/s)	v_j	21	21	21	21	21	21	21	21	21
Fuel jet velocity (m/s)	v_f	0.1	0.2	0.28	0.33	0.38	0.46	0.48	0.56	0.58
Coflow velocity (m/s)	v_c	5.5	5.5	5.5	5.5	5.5	5.5	5.5	5.5	5.5
Overflow equivalence ratio	ϕ[a]	0.008	0.015	0.021	0.025	0.029	0.035	0.036	0.042	0.044
Flame height (mm)	L_f	10	25	72	85	102	172	200	225	243

		F	Q	R	S
Panel c					
Microjet velocity (m/s)	v_j	21	21	21	21
Fuel jet velocity (m/s)	v_f	0.33	0.33	0.33	0.33
Coflow velocity (m/s)	v_c	5.5	2.17	0.74	0.36

Line missing

the jet fluid and the ambient fluid and in reacting cases, its affect on the residence time through the flame and the overall chemical reaction. According to their analysis, an enhanced entrainment of oxidizer leads to an increased reaction rate in an otherwise diffusion limited flame, and causes a reduction in flame height for a given fuel burning rate. Apart from the reduction of the flame height, the microjet flame also shows a radially compact structure which is also caused by the enhanced radial influx of the oxidizer.

A sudden change in the flame shape and luminosity is observed when v_f is increased from 20 m/s (Flame (E)) to 21 m/s (Flame (F)). The overall flame luminosity and the fluttering noise intensity decrease significantly. Flame (E) contains some yellow sooting portions, whereas Flame (F) is bright blue. The unconfined flames investigated by us previously did not exhibit such an abrupt change when the microjet velocity was increased. However, at the higher microjet velocity a confined flame is locally quenched along its centerline in a similar manner to an unconfined flame. In these flames Zone II is extinguished when $v_f > 21$ m/s, leaving a very unsteady Zone I and a flame that is truncated at the neck. The local strain rate is so high that, unlike in the Flames (C)–(F), reignition cannot occur at the neck and, as a result, the fluttering sound disappears, too. A considerable fraction of the fuel escapes unburned for such a flame, which is detrimental for single stage burners. However, the concept can be useful in sequential/cascaded combustors, such as next-generation gas turbines. Here, only partial burning of fuel is required in each stage with simultaneous dilution and premixing of the fuel and exhaust.

Schlieren images of microjet flame structures for Flames (B) and (F) are presented in Fig. 3. The Schlieren image for Flame (B) shows the presence of a cold weak microjet along the centerline. It does not yet have the strength to significantly alter the oxidizer entrainment. However, the corresponding image for Flame (F) is considerably different.

It clearly illustrates the two flame zones that are separated by the constricted neck. In Zone I, the flow is

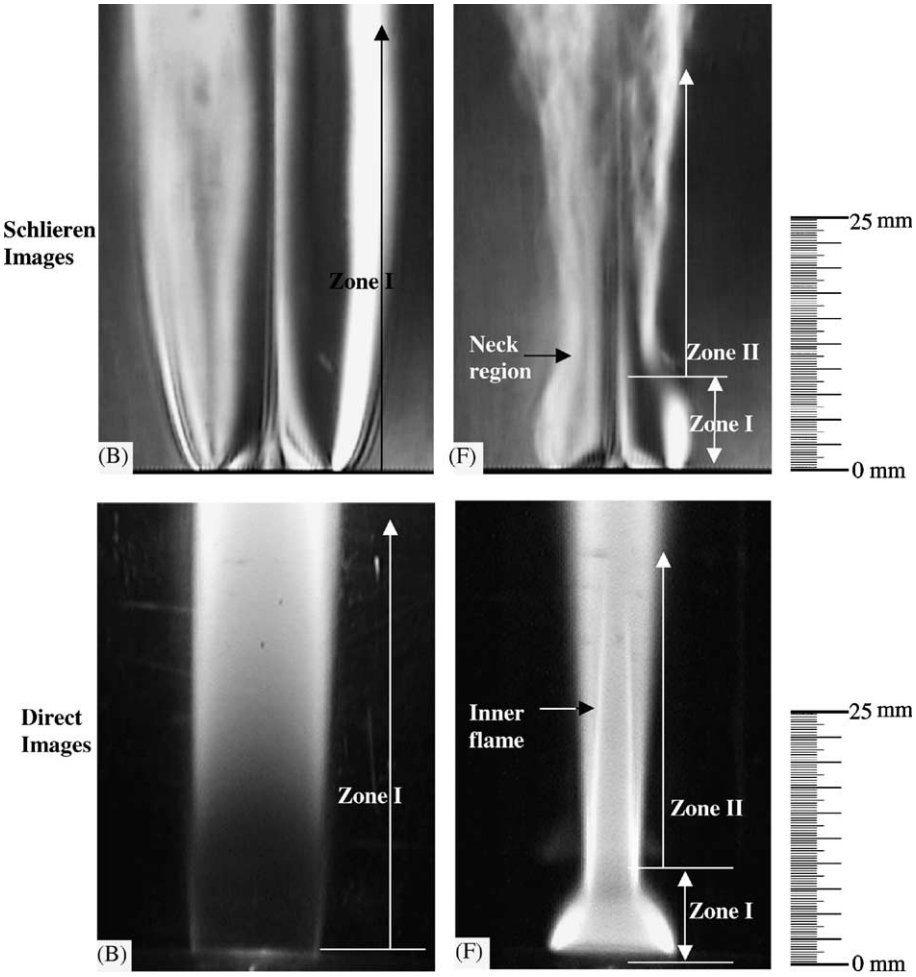

Fig. 3. Flame structure for two different microjet velocities (Flames (A) and (F) of Table 1(panel a)). Schlieren images (top) and corresponding direct images (bottom).

laminar and there is intense mixing at the neck, leading to the turbulence in Zone II. Shear layer instabilities produced by the high velocity ratio coaxial jets might lead to this turbulence. The image of Flame (F) also shows that an "inner" flame grows from the "neck" in the downstream region. Here, the microjet air leads to the formation of an additional inner nonpremixed flame interface.

The flame height increases when the fuel flowrate is augmented for constant microjet and coflow velocities. Fig. 4 presents images of Flames (G)–(O) (of Table 1(panel b)). Flames (G) and (H) have a truncated Zone II from which unreacted fuel escapes. For Flame (I), the "inner" flame adjacent to the microjet alone constitutes Zone II. The outer flame envelope reappears for Flame (F) as the fuel flowrate is increased. Further increase in the fuel flow elongates both Zones I and II. However, the inner flame cone height in Zone II remained constant for a given microjet flow rate. In all these cases the fuel burns without any noticeable soot formation. The burner power input varies over an order of magnitude from approximately 200 W in case (G) to 1000 W in case (O).

The corresponding variations of the heights of Zones I and II with respect to the fuel jet velocity and fuel jet Froude number (Fr_f) are presented in the inset in Fig. 4. Increasing the fuel velocity from 0.2 m/s to 0.28 m/s (Flames (I) and (F), respectively) results in the reappearance of Zone II and a ~300% increase in the total flame height $h(= h_1 + h_2$, i.e., the sum of the Zone I and II heights). The variation of h with the fuel flowrate can be represented by a second-order polynomial for a specified value of v_j (corresponding variation with Fr_f is merely its linear multiple). This dependence is unlike laminar ($h \propto$ fuel flowrate) or turbulent (for which h is independent of fuel flowrate) nonpremixed flame behavior. Therefore, for a microjet-assisted flame, h is more sensitive to the fuel flowrate than for laminar or turbulent nonpremixed flames. This feature is useful for the dynamic control of flame length in industrial applications such as material processing furnaces in which the load dimensions can vary considerably. In other applications, flame impingement on the combustor walls can be avoided using the technique.

Varying the coflow velocity has a weak influence on the height of microjet-assisted flames. For larger microjet velocities, a variation in the coflow velocity changes the characteristics of the flame neck. The faster the reignition occurs after local extinction at the neck, the more resistant Zone II is to external disturbances. Fig. 5 presents images of microjet-assisted flames established with different coflows (Flames (F) and (Q)–(S) of Table 1(panel c)). When the coflow is reduced below that of Flame (S), pockets of local extinction prevail long enough to extinguish the flame with the slightest perturbation. For all these flames the overall equivalence ratio is much smaller than unity. Hence the observed phenomenon is predominantly a hydrodynamic effect. For Flames (R) and (S) large dark areas appear in Zone II due to temporary local extinction. Therefore, the selec-

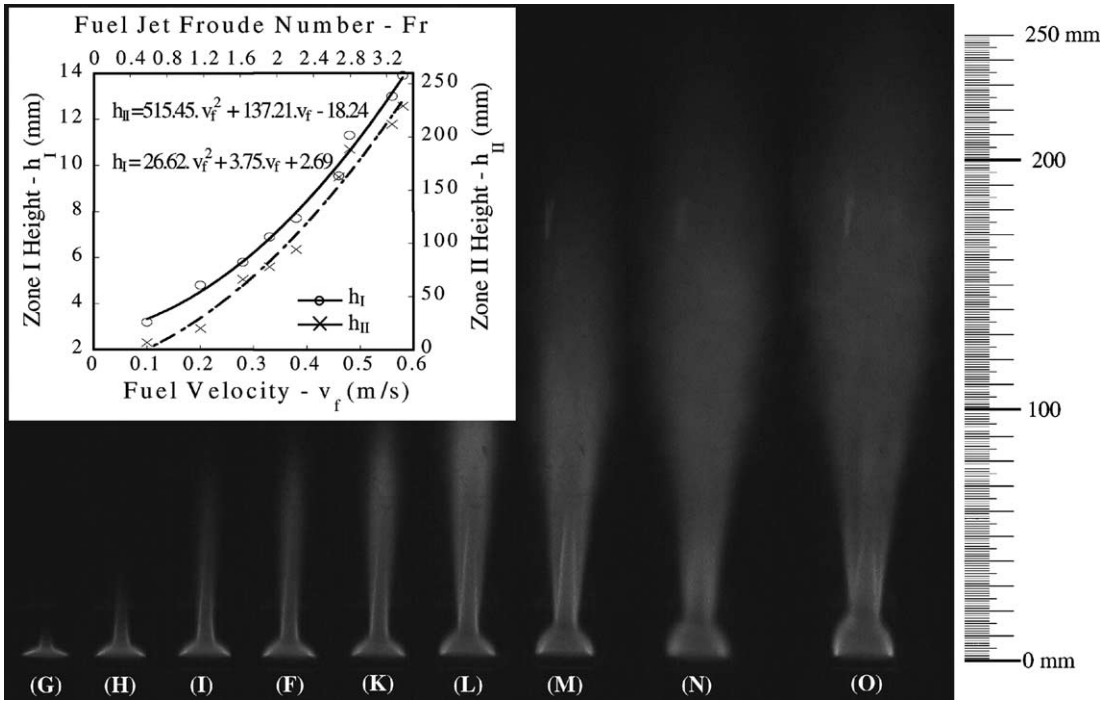

Fig. 4. Effects of varying the fuel velocity on microjet-assisted flame topologies. The flames correspond to the conditions of Table 1(panel b). Inset: the heights in Zones I and II of the flames as a function of fuel jet velocity (a scale for Fr_f is also included).

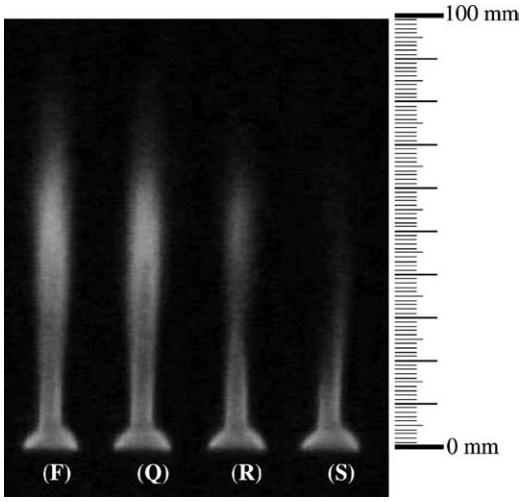

Fig. 5. Effects of varying coflow on the microjet-assisted flame structure.

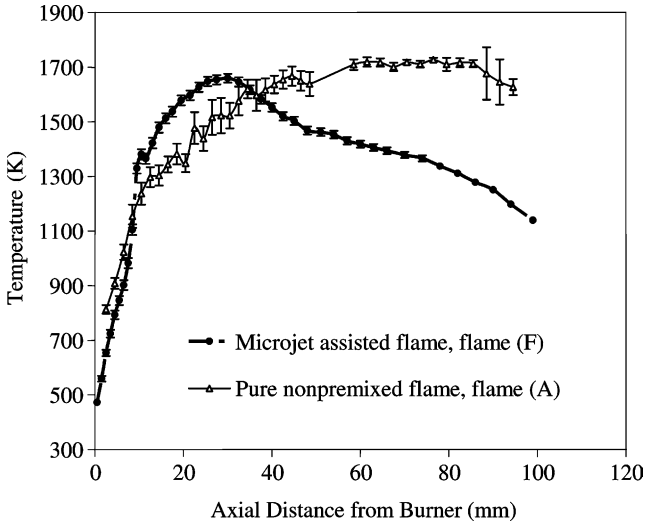

Fig. 7. Axial centerline temperature profile for a microjet-assisted flame and a corresponding conventional nonpremixed flame.

tion of a proper range of coflow velocities is important to maintain a stable flame.

The heights of the stable flames described in Table 1(panel a)–(panel c) are separately proportional to v_f^2, v_j^{-1} (the conventional nonpremixed Flame (A) is excluded from the analysis), and $v_c^{0.1}$. Thus, a velocity parameter $\Pi = v_f^2 v_c^{0.1}/v_j$ can be used to correlate the microjet assisted flame heights with all possible combinations of v_f, v_j, and v_c. Analysis of flames (D) through (O) yields a correlation for the Zone II width (w) with Π. These results are summarized in Fig. 6.

Fig. 7 presents the axial temperature distribution along the centerline of Flame (F). For comparison, the centerline temperature for the conventional nonpremixed flame (Flame (A)) is also presented. The burner exit temperature is lower for Flame (F) than for Flame (A) due to the advective cooling caused by the cold microjet air stream. However, the temperature rise for the microjet-assisted flame is steeper. Ganguly and Puri (2004) have shown that this larger temperature gradient is due to the enhanced oxidizer entrainment and, consequently, faster burning in a microjet-assisted flame. In Zone I of Flame (F), the radial heat flux from the flame surface towards the centerline increases with height as the reaction zone shifts inward. This causes a larger temperature gradient for the first 10 mm for which $dT/dz \sim 91$ K/mm as compared to ~48 K/mm for Flame (A). Downstream of the "flame neck", the outer reaction zone spreads radially outward, which leads to a reduction in this gradient (~16 K/mm from $z = 10$–27 mm). The peak flame temperature is, however, similar for both the microjet-assisted and conventional nonpremixed flames. Therefore, the microjet does not produce significant cooling, which would be detrimental to overall heat transfer.

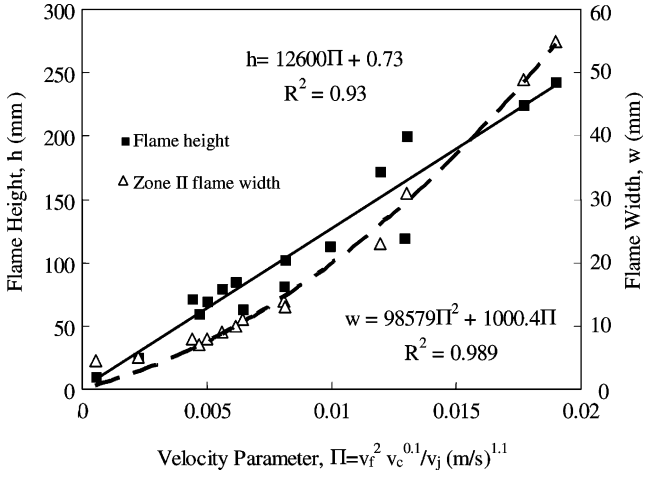

Fig. 6. Flame height and width correlated with the microjet (v_j), fuel jet (v_f) and coflow (v_c) velocities for the burner.

Fig. 8 presents NO_x and CO emissions from microjet assisted flames. Here, the fuel flow and coflow velocity are kept constant while v_j is increased. Both emissions are almost constant until $v_j \sim 21$ m/s (Flame F), and the CO, NO and NO_2 exhaust molar concentrations are ~1, 20, and 0.26 ppm, respectively for an O_2 concentration of ~20%. The figure indicates that flame shape control is feasible without an emissions penalty when the microjet velocities are restricted below a critical value. (Local extinction at the flame neck occurs beyond $v_j = 21$ m/s, which leads to a larger emitted CO fraction of 15.4 ppm for another 5 m/s increase in v_j. The NO_2 emission increases from ~0.3 ppm to 0.6 ppm as the flame is quenched and the lower overall temperatures lead to smaller NO_2 dissociation. Incomplete combustion also causes depletion in the radical pool and a corresponding reduction in the NO production.) Microjet

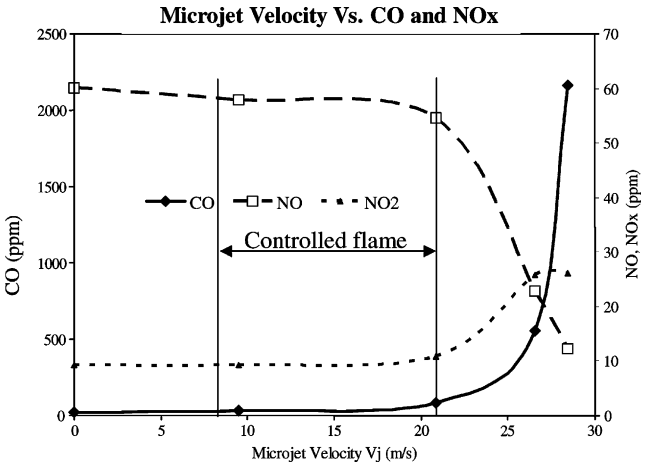

Fig. 8. Overall CO, NO and NO_2 emissions from microjet-assisted flames.

control is less flexible from the perspective of CO emissions than for NO_x control. However, in a multi-stage burner where CO reburning occurs, the microjet velocity could be maintained at higher values.

The results for the confined flames are in general agreement with our previous investigation that considered unconfined flames in the absence of a coflow. This is to be expected, since the coflow velocity has a weak influence on the neck structure and, as shown in Fig. 5, on the flame height. In order to further clarify the importance of the microjet hydrodynamics in altering the flame shape, we introduced an inert nitrogen microjet into an unconfined flame. Fig. 9(A)–(F) present images of flames with nitrogen microjets of varying velocities. The fuel and microjet velocities for each flame correspond to the respective cases of Table 1(panel a) (hence, Fig. 2) with the exception that that there is no coflow. The conventional nonpremixed flame in the absence of a coflow is taller than the same with coflow. However, the results are also relevant to confined flames. The topologies of the base of Flame (F) of Fig. 9 and of the base of its counterpart Flame (F) of Fig. 3 share a strong resemblance. Since the introduction of an inert gas such as nitrogen as the microjet fluid has a similar effect as air, which is an oxidizer, it is clear from the images that the primary influence of the microjet is of a hydrodynamic nature. Since the type of microjet fluid is not important in controlling flame shape and luminosity without cooling, these results show that it is possible to use exhaust combustion products or recirculation gas in an industrial application.

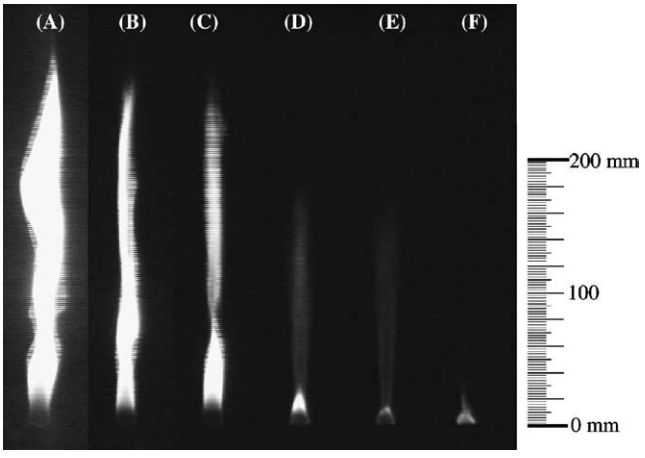

Fig. 9. Flame shape control for unconfined ($v_c = 0$) flames using nitrogen microjets. The fuel and microjet velocities for each flame correspond to the respective cases in Table 1(panel a).

5. Conclusions

An air microjet can be applied at the center of a nonpremixed flame to control the flame height and luminosity.

1. The microjet assisted flame consists of a laminar base (zone I) and a turbulent trail (zone II) that are separated by a "flame neck".
2. For specified microjet and coflow velocities, the flame height is more sensitive to the fuel flowrate than for laminar or turbulent nonpremixed flames.
3. Effective flame control is possible without an emissions penalty. The emissions from microjet-assisted flames are similar to those from a corresponding nonpremixed flame over a large range of microjet velocities that significantly alter the flame shape.
4. Although the flame topologies (and heat transfer characteristics) of microjet-assisted flames are considerably different from those of conventional nonpremixed flames, the peak flame temperatures are similar.
5. This control strategy can also be achieved by using a chemically inert microjet fluid.

The study addresses the parametric variations by altering the fuel, microjet and the coflow velocities for a burner with an input power of the order of 1 kW and smaller. This power range is of direct relevance to *miniaturized combustion devices* and pilot scale flames. However, before implementing microjet flame control for large scale industrial burners, a separate parametric investigation that addresses the effect of different burner sizes and aspect ratios of the microjet to fuel jet or coflow jet dimensions is required.

References

Azzoni, R., Ratti, S., Puri, I.K., Aggarwal, S.K., 1999. Gravity effects on triple flames: Flame structure and flow instability. Phys. Fluids 11, 3449–3464.

Ban, H., Venkatesh, S., Saito, K., 1994. Convection-diffusion controlled laminar micro flames. ASME J. Heat Tr. 116, 954–959.

Becker, H.A., Liang, D., Downey, C.I., 1981. Effect of burner orientation and ambient airflow on geometry of turbulent free diffusion flames. Proc. Combust. Inst. 18, 1061–1071.

Becker, H., Yamazaki, S., 1978. Entrainment, momentum flux and temperature in vertical free turbulent diffusion flames. Combust. Flame 33, 123–149.

Ganguly, R., Puri, I.K., 2004. Nonpremixed flame control with microjets. Expts. Fluids 36 (4), 635–641.

Hamins, A., Yang, J.C., Kashiwagi, T., 1992. An experimental investigation of the pulsation frequency of flames. Proc. Combust. Inst. 24, 1695–1702.

Han, D., Mungal, M.G., 2001. Direct measurement of entrainment in reacting/nonreacting turbulent jets. Combust. Flame 124 (3), 370–386.

Hanus, F., Hubo, R., 1999. Flame straightening of thermomechanically rolled structural steel. Steel Res. 70, 193–197.

Hertzberg, J.R., 1977. Conditions for a split diffusion flame. Combust. Flame 109, 314–322.

Kimura, I., 1965. Stability of laminar jet flames. Proc. Combust. Inst. 10, 1295–1300.

Lawton, J., Weinberg, F.J., 1969. Electrical Aspects of Combustion. Clarendon Press, Oxford.

Pesenti, B., Meunier, H., 2000. Effect of swirl intensity on a variable flame length gas burner performance. Euro. J. Mech. Environ. Eng. 45, 19–27.

Roper, F.G., 1977. The prediction of laminar jet diffusion sizes: part-I. Theoretical model. Combust. Flame 29, 219–226.

Roper, F.G., Smith, C., Cuningham, A.C., 1977. The prediction of laminar jet diffusion flame sizes: Part-II. Experimental verification. Combust. Flame 29, 227–234.

Thring, M.W., Newby, M.P., 1953. Combustion length of enclosed trubulent diffusion jet flames. Proc. Combust. Inst. 4, 789–796.